PHYSICAL REVIEW D **88,** 094005 (2013)

Quark matter under strong magnetic fields in SU(2) NJL-type models: Parameter dependence of the cold dense matter phase diagram

Pablo G. Allen[1] and N. N. Scoccola[1,2,3]

[1]*Physics Department, Comisión Nacional de Energía Atómica, Avenida Libertador 8250, 1429 Buenos Aires, Argentina*
[2]*CONICET, Rivadavia 1917, 1033 Buenos Aires, Argentina*
[3]*Universidad Favaloro, Solís 453, 1078 Buenos Aires, Argentina*

(Received 11 September 2013; published 12 November 2013)

The phase structure of magnetized cold quark matter is analyzed in the framework of the two-flavor Nambu-Jona-Lasinio models paying special attention to its dependence on the model parameters as different values within the phenomenological allowed range are considered. We first discuss the simpler chiral limit case, and then the more realistic situation of finite current masses. We show that in spite of the difference in the nature of some transitions, both cases are alike and exhibit a rather rich phase structure for a significant range of acceptable parameters. A simplification of the phase structure is obtained as parameters leading to larger values of the dressed quark mass in the vacuum are considered. Finally, we consider the so-called ''inverse catalysis effect'' showing that in some phases it implies an actual decrease of the order parameter as the magnetic field increases.

DOI: 10.1103/PhysRevD.88.094005 PACS numbers: 24.10.Jv, 25.75.Nq

I. INTRODUCTION

Understanding the behavior of strongly interacting matter under the influence of intense magnetic fields has become an issue of increasing interest in recent years [1]. This has been mostly motivated by the realization that strong magnetic fields may be produced in several physically relevant situations. For example, present estimates [2] indicate that in noncentral heavy ion collisions at very high energies the field intensity could be $B \sim 10^{19}$ G, i.e. $eB \sim 0.06$ GeV^2 in natural units. Moreover, the compact stellar objects believed to be the source of intense γ and X rays, magnetars, are expected to bear fields of the order of 10^{13}–10^{15} G at their surface reaching values several orders of magnitude greater at their center [3]. Note that in all these situations the matter is, in addition, subject to extreme conditions of temperature and/or density. Thus, it is of great interest to investigate which modifications are induced by the presence of strong magnetic fields on the whole QCD phase diagram. Unfortunately, even in the absence of those fields, the present knowledge of such phase diagram is only schematic. Only recently have powerful lattice QCD (LQCD) simulations [4] firmly established that for $2 + 1$ flavors and vanishing baryon chemical potential there is a crossover-like transition at $T_{pc} \simeq 160$ MeV from a hadronic phase, in which chiral symmetry is broken and quarks are confined, to a partonic phase in which chiral symmetry is restored and/or quarks are deconfined. The situation is less clear for finite chemical potentials due to the well-known difficulty given by the so-called sign problem which affects lattice calculations [5]. Of course, the presence of strong magnetic fields makes the situation even more complex. Thus, most of our present knowledge of their effect comes from investigations performed in the framework of effective models (see e.g. Refs. [6,7] and references therein). A general outcome is an enhancement at vanishing chemical potential of the dynamical symmetry breaking due to external magnetic field, a phenomenon usually referred to as ''magnetic catalysis'' [8]. In fact, a recent LQCD study [9] of the behavior of the u- and d- condensates at zero and finite temperature in an external magnetic field has confirmed the magnetic catalysis phenomena predicted by most of the models at zero temperature. However, for temperatures of the order of the crossover temperature a decrease of the quark condensates is found. It remains an open and interesting question what prevents magnetic catalysis to persist for these larger temperatures. In this article we will concentrate on a different sector of the phase diagram: that of finite chemical potential and low temperatures. Although this region has been the subject of several investigations in the past (see e.g. Refs. [10–18]), as in the case of vanishing magnetic field the corresponding behavior of the strongly interacting matter has not been firmly established. For example, only very recently was it fully realized that there exists an ''inverse catalysis effect'' at certain values of the magnetic field [19]. We will perform our analysis in the framework of the two-flavor Nambu-Jona-Lasinio (NJL)-type models [20]. As is well known (see e.g. Ref. [21]), even in the simplest version of these models there is a significant range of phenomenologically acceptable values for the model parameters. In this situation, previous NJL studies of the effect of the magnetic field on cold quark matter have only considered some particular choices of allowed parameterizations. Our aim is to perform a systematic analysis of how both the qualitative and quantitative details of the phase diagram of cold dense quark matter subject to intense magnetic fields depend on the specific choice of the parameters. It should be noted that the generic features of such phase diagram have been first studied in Refs. [10,11]. However, in these works only the

chiral limit was considered and no details of the precise dependence of the phase diagram on parametrizations within the range of phenomenological interest were given. As already mentioned, for the more realistic case of finite current quark masses only a few particular parametrizations were considered.

This work is organized as follows. In Sec. II we provide a brief review of the NJL model description of cold dense quark matter in the presence of external magnetic fields. The model parameters, as well as the way to determine them, are also introduced. In Sec. III we consider the parameter dependence of the phase diagrams in the chiral limit. The case of finite quark masses is analyzed in Sec. IV. Our main conclusions are presented in Sec. V. Finally, we have included two appendices: in Appendix A we provide some details of the parametrizations for the chiral case while in Appendix B we give the numeric values of parameters used for the case of finite current masses.

II. FORMALISM

Our starting point is the Euclidean effective action of the SU(2) NJL model in the presence of an external electromagnetic field. It reads:

$$S_E = \int d^4x\{\bar{\psi}(-i\gamma^\mu D_\mu + m_c)\psi - G[(\bar{\psi}\psi)^2 + (\bar{\psi}i\tau\gamma_5\psi)^2]\}, \quad (1)$$

where m_c is the current quark mass (we work in the isospin limit $m_c = m_u = m_d$) and G is a coupling constant. The coupling of the quarks to the electromagnetic field $\mathcal{A}_\mu$ is implemented through the covariant derivative $D_\mu = \partial_\mu - iq_f\mathcal{A}_\mu$ where q_f represents the quark electric charge ($q_u/2 = -q_d = e/3$). We consider a static and constant magnetic field in the z direction, $\mathcal{A}_\mu = \delta_{\mu 2}x_1 B$. Since the model under consideration is not renormalizable, we need to specify a regularization scheme. Here, we introduce a sharp cutoff in 3-momentum space, only for the ultraviolet divergent integrals. Together with m_c and G, the cutoff Λ forms a set of three parameters that completely determine the model. These parameters are usually fixed so as to reproduce the empirical values in the vacuum of the pion mass m_π, the pion decay constant f_π, and the quark condensate $\langle\bar{q}q\rangle_0$. The latter is related to dressed quark mass in the vacuum M_0 via $M_0 = m_c - 2G\langle\bar{q}q\rangle_0$. Whereas the physical values $m_\pi = 138.0$ MeV and $f_\pi = 92.4$ MeV are known quite accurately, the uncertainties for the quark condensate are rather large. Limits extracted from sum rules are 190 MeV $< -\langle u\bar{u}\rangle_0^{1/3} <$ 260 MeV at a renormalization scale of 1 GeV [22], while typical lattice calculations yield $-\langle u\bar{u}\rangle_0^{1/3} = 231 \pm 8 \pm 6$ MeV [23] (see e.g. Ref. [24] for some other lattice results). As a consequence of this, different parametrizations compatible with this rather broad range of values for the condensate have been used in the literature. As frequently done, here we choose to take M_0 as the quantity which defines those parametrizations. To be compatible with the above-mentioned phenomenological values for the quark condensate we must have $300 \lesssim M_0 \lesssim 600$ MeV [21].

To account for finite temperature T and chemical potential μ one can follow the standard Matsubara formalism which amounts to performing the replacements,

$$p_4 \to (2n+1)\pi T - i\mu; \qquad \int \frac{dp_4}{2\pi} \to \sum_n. \quad (2)$$

In the case of the local NJL model under consideration the sum over Matsubara modes can be analytically performed. Since we are particularly interested in analyzing the behavior of cold quark matter, we take the limit of vanishing temperature in the resulting expressions. In this limit, the thermodynamical potential in the mean field approximation (MFA) reads [11,13]

$$\Omega(\mu,B,M) = \frac{(M-m_c)^2}{4G} + \frac{N_c N_f}{8\pi^2}\left\{M^4\ln\frac{\Lambda+\sqrt{\Lambda^2+M^2}}{M} - \Lambda(2\Lambda^2+M^2)\sqrt{\Lambda^2+M^2}\right\}$$
$$- \frac{N_c}{2\pi^2}\sum_{f=u,d}(q_f B)^2\left[\zeta'(-1,x_f) + \frac{x_f^2}{4} - \frac{1}{2}(x_f^2 - x_f)\ln x_f\right]$$
$$- \frac{N_c}{4\pi^2}\sum_{k,f}\theta(\mu - s_{kf})\alpha_k|q_f|B\left\{\mu\sqrt{\mu^2 - s_{kf}^2} - s_{kf}^2\ln\left[\frac{\mu+\sqrt{\mu^2-s_{kf}^2}}{s_{kf}}\right]\right\}, \quad (3)$$

where $\alpha_k = 2 - \delta_{k0}$, $s_{kf} = \sqrt{M^2 + 2k|q_f|B}$ and $x_f = M^2/(2|q_f|B)$. In addition, $\zeta'(-1,x_f) = d\zeta(z,x_f)/dz|_{z=-1}$, where $\zeta(z,x_f)$ is the Riemann-Hurwitz zeta function. The sum over k in the last line corresponds to the sum over the populated Landau levels (LL's) associated to each quark flavor f. The dressed quark mass $M(\mu,B)$ at a given value of μ and B is found as solution of the gap equation, $\partial\Omega/\partial M = 0$. As is well known, the behavior of these solutions as a function of μ indicates the existence of some kind of phase transition which, in the chiral case, can be of first or second order depending on the value of the external magnetic field. For finite current masses, however,

these possible second order phase transitions become smooth crossovers. Consequently, there is not a unique way to define their position. In fact, even in the absence of a magnetic field, different prescriptions have been used in the literature to define the position of a crossover-type transition. They include, for example, the location of the peak of the chiral susceptibility $\chi_{\rm ch} = \partial\langle\bar{q}q\rangle/\partial m_c$, of the peak of the derivative of an order parameter with respect to some thermodynamical variable (as e.g. μ or T), etc. This issue will be discussed in some detail in Sec. IV. We should also mention that, as will be seen in Sec. III, some additional second order transitions can occur in the chirally restored phase $M = 0$ in the chiral case. There, one should consider some additional quantity, like the quark number density $\rho = -\partial\Omega/\partial\mu$, in order to observe their effect.

As already stated, the main aim of this work is to perform a detailed analysis of how the character and location of these different types of phase transitions depend on the chosen parametrization of the NJL model. For convenience, we discuss in the next section the simplified case of $m_c = 0$. The more realistic case of finite quark mass will be addressed in Sec. IV.

III. PHASE DIAGRAMS IN THE CHIRAL LIMIT

In this section we analyze the chiral case $m_c = 0$. As discussed in the Appendix A, in this case the model has only two parameters: the coupling constant G and the 3D cutoff Λ. In order to work along a line of "constant physics" we determine them as a function of M_0 so as to reproduce a value of the pion decay constant in the chiral limit $f_\pi^{\rm ch} = 90$ MeV. The numerical results for the dimensionless coupling constant $g = G\Lambda^2$ and Λ as functions of M_0 are given in the Appendix A (see upper panel of Fig. 15). Note that since for $m_c = 0$ the pion decay constant is the only dimensionful quantity in the problem, any dimensionful quantity (expressed in natural units) has to be the product of some $f_\pi^{\rm ch}$-independent constant multiplied by some power of it. In this way, all the results to be shown in this section can be easily made "universal," in the sense of being independent of the chosen value for $f_\pi^{\rm ch}$. Of course, some extra dependence on the chosen procedure to regularize the UV divergencies might still exist.

We start by discussing the situation at vanishing magnetic field. Although this has already been discussed in the literature to some extent [25–27] it will serve as a benchmark for a better understanding of the modifications introduced by the presence of external magnetic fields. The corresponding diagram in the M_0-μ plane is shown in Fig. 1. There, the full lines correspond to first order phase transitions while the dashed lines to second order ones. Let us recall that each value of M_0 corresponds to a different parametrization of the model. As we see, depending on the value of M_0, three different regions can be distinguished. For $M_0 < M_0(b)$ two consecutive second order transitions occur as μ increases. The first one connects a phase in

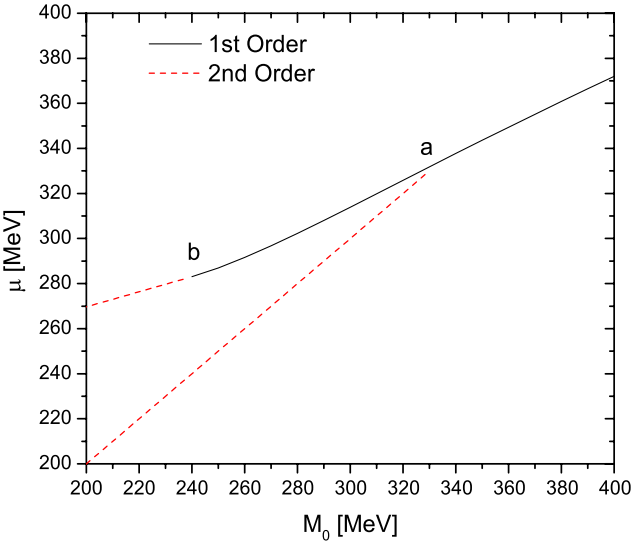

FIG. 1 (color online). Critical chemical potentials as functions of the model parametrization (specified by the value of M_0) in the absence of the magnetic field.

which $M = M_0$ independently of the value μ to one in which $M = M(\mu, 0)$ with $0 < M < M_0$. The second transition in turn connects the latter phase to the chirally restored phase $M = 0$. Note that while the first of these transitions implies a discontinuity of $d^2M/d\mu^2$ at the critical point [26], in the case of the second one already the first derivative is discontinuous at the corresponding point. For $M_0(b) < M_0 < M_0(a)$ the situation is similar except for the fact that the second transition is of first order type. Finally, for $M_0 > M_0(a)$ there is only one first order transition connecting the phase with $M = M_0$ to the one with $M = 0$. These possible situations are illustrated in Fig. 2 where we display the behavior of M (upper panel) and the density ρ (lower panel) as a function of μ for three values of M_0, each one lying in one of the above-mentioned regions. For our chosen value of $f_\pi^{\rm ch}$ we obtain $M_0(a) = 334.45$ MeV and $M_0(b) = 239.64$ MeV. As already indicated, these quantities can be written in a "universal" way if we express them in terms of $f_\pi^{\rm ch}$. We obtain

$$M_0(a) = 3.716 f_\pi^{\rm ch}; \qquad M_0(b) = 2.663 f_\pi^{\rm ch}. \tag{4}$$

It should be mentioned that an approximation to the above expression for $M_0(a)$ was given in Ref. [25] where the relation $M_0(a) \simeq 4 f_\pi^{\rm ch}$ was quoted. On the other hand, in Ref. [11] the values of $M_0(a)$ and $M_0(b)$ were given in terms of the cutoff Λ. Although in principle correct, we find that this way to express these critical masses might be somewhat inconvenient. Note that for a fixed ratio M_0/Λ, different values of Λ correspond to different values of $f_\pi^{\rm ch}$ [see Eq. (A2)] and, thus, do not represent the same physical situation. For this reason we find it more adequate to take $f_\pi^{\rm ch}$ instead of Λ as the "independent" variable.

We turn now to the finite B case. In Fig. 3 we display the behavior of the critical chemical potentials of the different

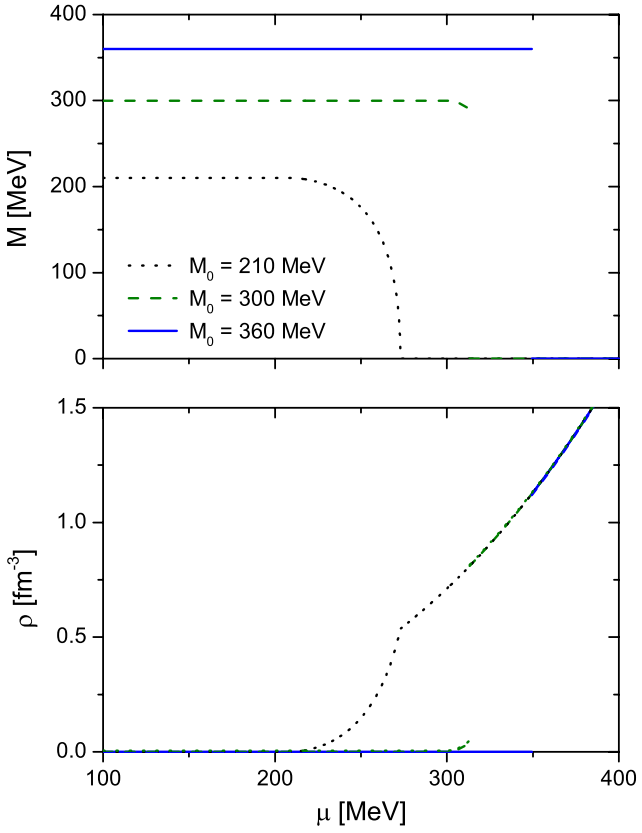

FIG. 2 (color online). Behavior of the dressed mass M (upper panel) and the quark density ρ (lower panel) for $eB = 0$. Plots for several representative model parameter sets specified by the value of M_0 are shown.

possible transitions as functions of M_0 for several representative values of eB. Note again that if the values of μ, M_0 and eB are scaled with the corresponding powers of $f_\pi^{\mathrm{ch}} = 90$ MeV these figures are "universal" in the sense described above. We concentrate first in the lowest value of the magnetic field considered, $eB = 0.01$ GeV^2. Comparing it with the corresponding one for $eB = 0$ shown in Fig. 1, we observe some differences and similarities. First, here we can observe that there is a clearly different behavior depending on whether $M_0 > M_0(a)$ or not. Note that in general the value of $M_0(a)$ depends on eB (see Fig. 5 below and its corresponding discussion). For parametrizations with $M_0 > M_0(a)$ there is only one first order transition at a given critical μ. Such transition connects the chirally broken phase with $M = M(0, B)$ to the chiral phase $M = 0$. On the other hand, for $M_0 < M_0(a)$ the chirally restored phase is reached only after a succession of several first order transitions. This situation is illustrated in the left panels of Fig. 4 where we display the behavior of M (upper panel) and the quark density ρ (lower panel) for $eB = 0.01$ GeV^2 and two representative values of M_0. It is interesting to analyze the case $M_0 < M_0(a)$ in some detail. Contrary to what happens for $eB = 0$, where the lowest critical μ corresponds to a second order transition, we note that as soon as a small external field is present such transition becomes first order. It is possible to check that if one takes, for example, $M_0 = 210$ MeV and considers values of $eB < 0.01$ GeV^2, the number of first order transitions needed to reach the $M = 0$ phase increases as eB decreases and, eventually, the curves of M and ρ as functions of μ tend to those shown in Fig. 2 as eB vanishes. It is clear that the discontinuities present in the finite eB case are due to the quantization of the (Landau) levels induced by the magnetic fields. Another important observation concerns the last transition before the $M = 0$ phase is reached. Such transition can be of first or second order depending on the chosen value of M_0. Although somewhat difficult to observe in the case of $eB = 0.01$ GeV^2, this effect becomes clear as larger values of eB are considered. Finally we note that, independently of the chosen parametrization, in the chirally restored phase $M = 0$ extra second order transitions occur at the chemical potentials indicated by the dotted lines. The corresponding critical values of μ are such that some new Landau levels contribute to the last line of Eq. (3) for $M = 0$. Thus,

$$\mu = \sqrt{2kc_f eB/3} \tag{5}$$

where $c_u = 2c_d = 2$. It is important to note that, although in the chiral case these transitions do not cause any change in the chiral order parameter, some other quantities like the derivatives of the quark density do display discontinuities at the critical point. This effect can be observed, for example, in the behavior of the density as function of μ for the case $M_0 = 210$ MeV displayed in the left lower panel of Fig. 4. In fact, all the features present there are associated with the magnetic oscillations related to the so-called "van Alphen–de Haas effect" [10]. Note that while for chemical potentials leading to massive phases these oscillations induce first order transitions, for those corresponding to massless ones the transitions are of second order.

Continuing with the analysis of the M_0-μ diagrams displayed in Fig. 3 we discuss now how they are modified as eB increases. We see that for $eB = 0.05$ GeV^2 the value of $M_0(a)$ is somewhat larger than for $eB = 0.01$ GeV^2. In addition, for a given $M_0 < M_0(a)$ the number of first order transitions needed to go from the $M = M(0, B)$ phase to the one with $M = 0$ decreases. Of course, as is clear from Eq. (5), the spacing between the dotted lines becomes larger. Note also that, for the range of values of M_0 considered, all the transitions connecting the finite M phases to the vanishing M ones are of first order type. The situation changes for $eB = 0.08$ GeV^2 since in this case there is a region of values of M_0 for which the $M = 0$ phase is reached through a second order phase transition. It is interesting to note that such second order line ends at the point where a dotted line meets a first order line. As seen in previous cases, however, the intersection of a dotted line

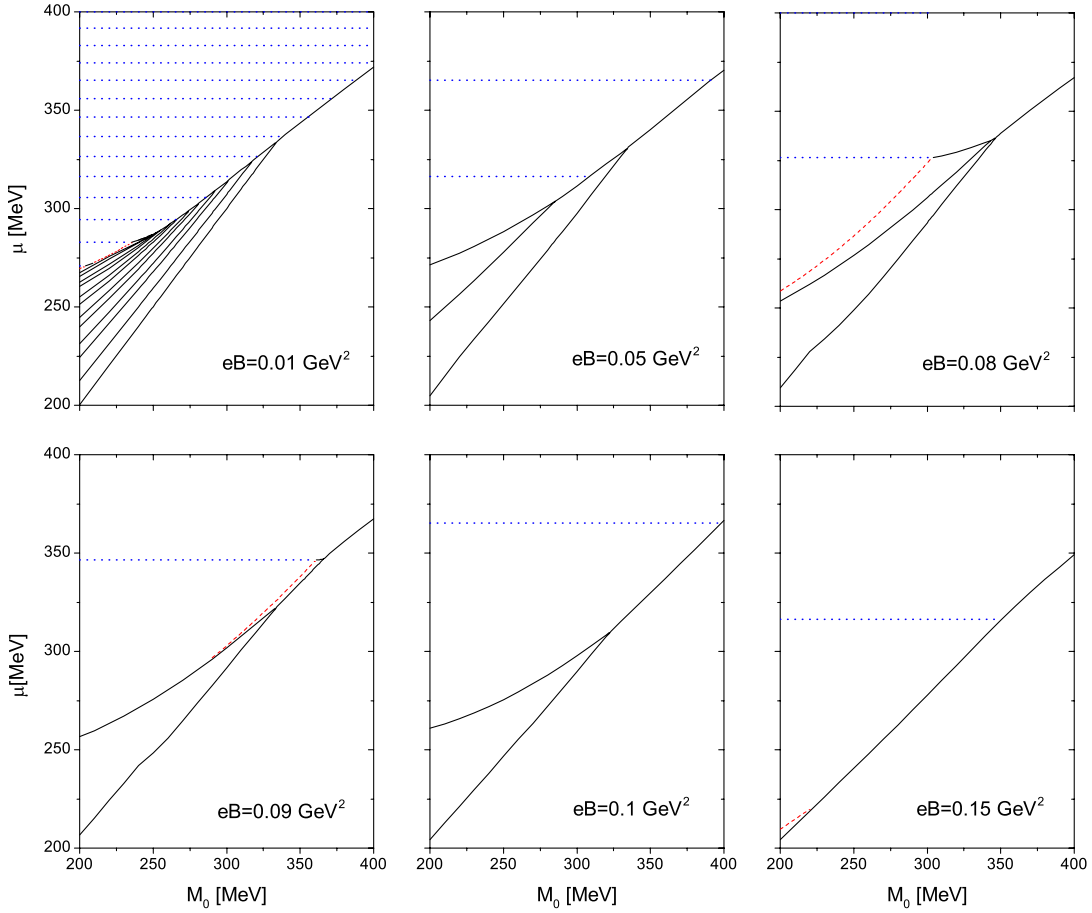

FIG. 3 (color online). Critical chemical potentials as functions of the model parametrization specified by the value of M_0 for several representative values of the magnetic field.

and a first order one does not necessarily imply the existence of a second order "chiral" line that ends at the meeting point. The behavior of M and ρ as functions of μ for some representative values of M_0 are shown in the right panels of Fig. 4. For the next value considered, $eB = 0.09$ GeV^2, we observe that the point a still moves towards larger values of M_0, and both the beginning and the end of the second order line are inside the considered range of parametrizations. However, if we increase the magnetic field further to $eB = 0.10$ GeV^2 the position of a displays a sudden jump toward smaller values of M_0. Moreover, no second order "chiral" line is present for $M_0 > 200$ MeV. In the last case explicitly considered, which corresponds to $eB = 0.15$ GeV^2, we see that the point a has moved further to the lower left corner of the diagram. In addition a new second order line appears, but only for parametrizations corresponding to small values $M_0 < 220$ MeV. We note that for even larger values of eB we get $M_0(a) < 200$ MeV and, thus, there is only one first order transition in the whole range of parametrizations considered. Of course, in addition to such transition, there also exist the corresponding second order transitions which are always present in the chirally restored phase.

From the analysis above it is clear that the presence of the magnetic field induces a rather rich and diverse structure of phase transitions for the different possible parametrizations laying within the physical range $300 \lesssim M_0 \lesssim 600$ MeV. Particularly interesting is the behavior of the position of the critical point a as a function of eB. In fact, for parametrizations with $M_0 > M_0(a)$ only one first order phase transition connects the vacuum phase to the chirally restored phase. Such behavior is shown in Fig. 5. As we see, the corresponding curve is not monotonic and presents two peaks followed by two associated discontinuities. Expressed in "universal" fashion the highest maximum (hm) corresponds to

$$M_0(a)^{\mathrm{hm}} = 4.127 f_\pi^{\mathrm{ch}} \quad \text{with} \quad eB^{\mathrm{hm}} = 11.35 (f_\pi^{\mathrm{ch}})^2 \tag{6}$$

while the lowest maximum (lm) corresponds

$$M_0(a)^{\mathrm{lm}} = 3.798 f_\pi^{\mathrm{ch}} \quad \text{with} \quad eB^{\mathrm{lm}} = 17.95 (f_\pi^{\mathrm{ch}})^2 \tag{7}$$

which for our chosen value $f_\pi^{\mathrm{ch}} = 90$ MeV leads to $M_0(a)^{\mathrm{hm}} = 371.46$ MeV and $M_0(b)^{\mathrm{lm}} = 341.80$ MeV. We should mention that, in principle, additional peaks and discontinuities might appear for larger values of eB.

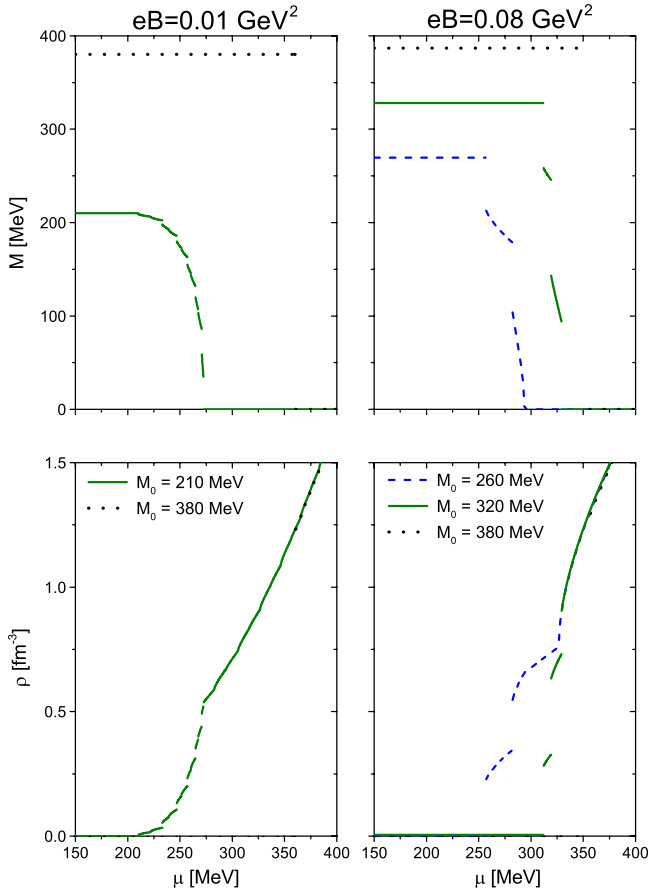

FIG. 4 (color online). Behavior of the dressed mass M (upper panels) and the quark density ρ (lower panels) for two selected values of eB and several representative model parameter sets specified by the value of M_0.

However, the corresponding values of $M_0(a)$ would be below 200 MeV and, thus, far from the physical range of interest. The value of $M_0(a)^{\rm hm}$ is particularly important. In fact, for parametrizations with $M_0 > M_0(a)^{\rm hm}$ the phase diagram in the eB-μ plane is very simple since, as it will be shown below, it only displays a single first order phase transition for all values of the magnetic field. It is interesting to note that the interval $M_0(a_{eB=0}) < M_0 < M_0(a)^{\rm hm}$ is the one mentioned in footnote 9 of Ref. [11] for which stable quark droplets are formed by massive quarks. Note, however, that no precise value for $M_0(a)^{\rm hm}$ was given in that reference.

We turn now to the analysis of the eB-μ phase diagrams. However, before considering values of M_0 within the accepted range of physical interest, we will focus on the situation for $M_0 = 200$ MeV. Although this might be only considered a case of academic interest, it is nevertheless instructive since it displays the full complexity that a phase diagram of this type might have, allowing also to appreciate how such diagram is simplified as M_0 increases towards the physical region of parameters. The corresponding phase diagram is shown in Fig. 6. This diagram

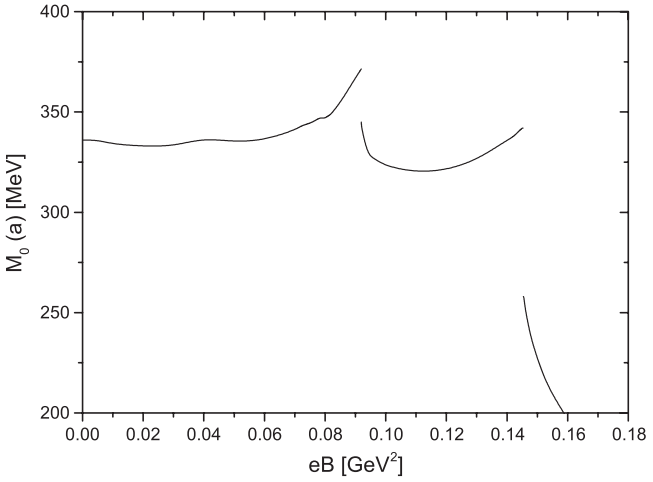

FIG. 5. Position of the critical point a as a function of eB in the chiral case. Note that for parametrizations with $M_0 > M_0(a)$ only one first order transition connects the vacuum phase to the chirally restored phases.

is very similar to the one sketched in Fig. 4 of Ref. [10] which corresponds to a simplified one-flavor model. Note that we use different types of lines to represent the various types of transitions. In Fig. 6, full (black) lines correspond to first order phase transitions, dashed (red) lines to second

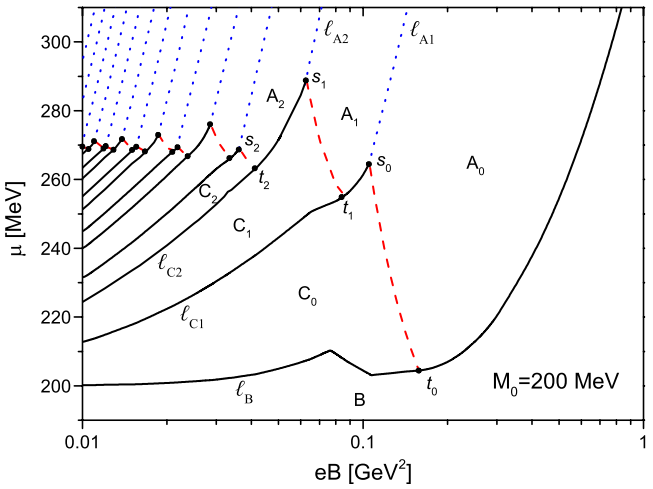

FIG. 6 (color online). Phase diagrams in the eB-μ plane for the chiral case and $M_0 = 200$ MeV. Full (black) lines represent first order phase transitions while dashed (red) lines represent second order ones. Dotted (blue) lines correspond to the second order transitions which separate the different massless phases. Phase B corresponds to the fully chiral symmetry broken phase with no LL populated, while the phases C_i to massive phases in which LL's up to $k = i$ for d-quarks and $k = m$ for u-quarks are populated. Here, $m = i/2((i-1)/2)$ if m is even (odd). In phase B, the dressed mass takes the vacuum value $M(0, eB)$ independently of μ while in the phases C_i it takes a smaller value which does depend on μ. The phases A_i are phases in which chiral symmetry is restored and LL's up to k (related to i as above) are populated.

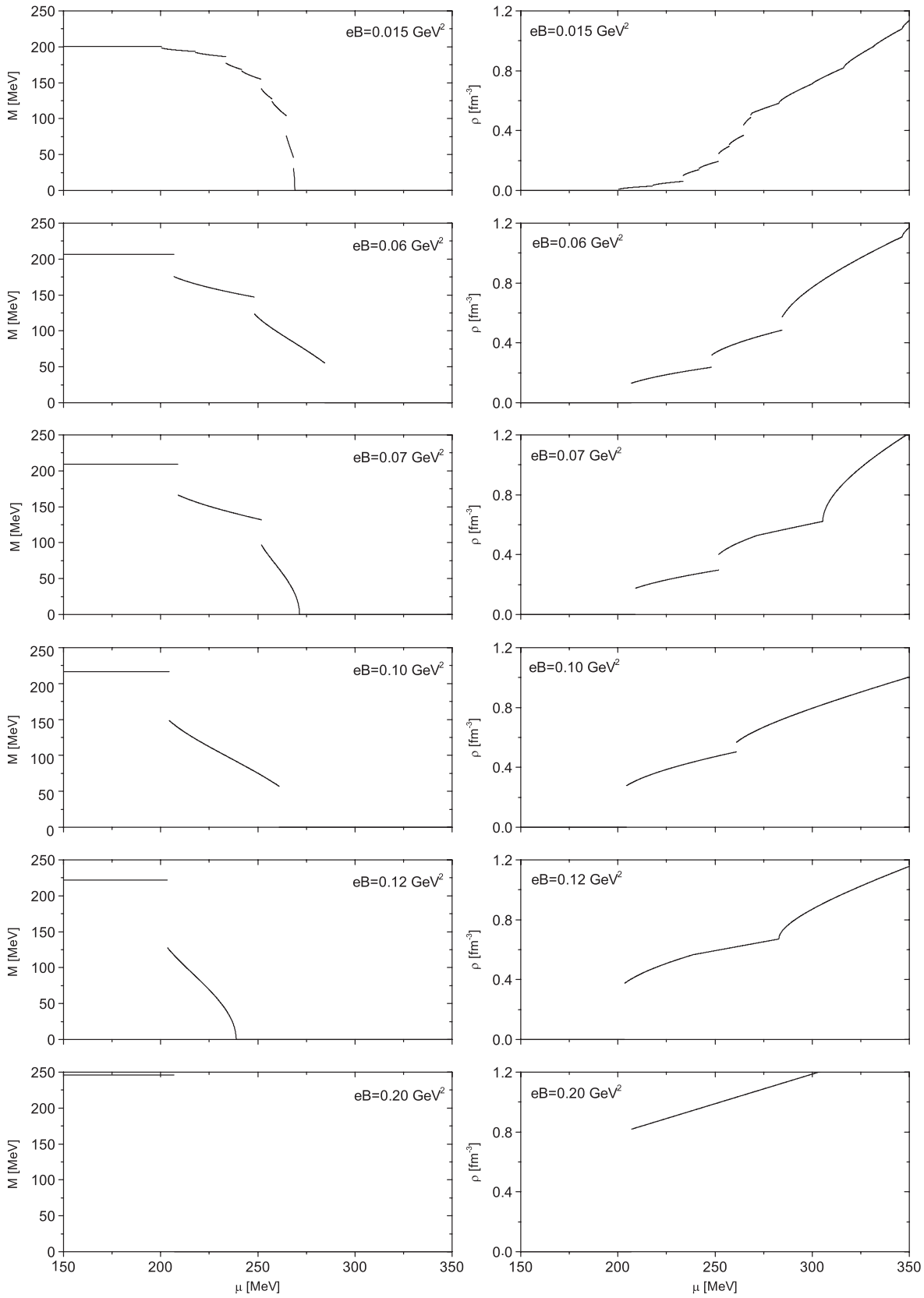

FIG. 7. Behavior of the dressed mass M (left panels) and the quark density (right panels) as functions of the chemical potential for the chiral case with $M_0 = 200$ MeV and several representative values of the magnetic field.

order "chiral" transitions and dotted (blue) lines to the second order transitions between massless phases. On the other hand we follow the notation of Ref. [10] to denote the different phases and critical points. In fact, the phase B corresponds to the fully chirally broken phase where $M = M(0, B)$, while the phases C_i correspond to massive phases where M also depends on μ. This can be clearly observed in Fig. 7 where we display the behavior of M (left panels) and ρ (right panels) for different representative values of eB. Note that while the quark density in the B phases vanishes, this is not the case in the phases C_i. Finally, the phases A_i correspond to massless phases with different number of populated LL's. For convenience, we also introduce the following notation for the lines separating the different phases. We use ℓ_B to indicate the first order line that separates the B phase from the C_0 or A_0 phases, ℓ_{Ci} (with $i = 1, 2\ldots$) the first order line separating the C_i and C_{i-1} phases and ℓ_{Ai} (with $i = 1, 2\ldots$) the second order line separating the A_i and A_{i-1}. Note, however, that in general there exists a segment of the ℓ_{Ci} line (that going from t_i to s_{i-1}) that actually separates the A_i and C_{i-1} phases. As discussed in Ref. [10], for vanishing eB all the ℓ_{Ci} lines are expected to meet ℓ_B at a single point, M, with $\mu(\mathrm{M}) = M = 200$ MeV in the present case. Note that this point should lie on the lower dashed line of Fig. 1 and, thus, corresponds to a second order transition point. The main difference with Fig. 4 of Ref. [10] is the form of the segments connecting the points t_i and s_{i-1}. In fact, we find that the slope of the corresponding functions $\mu(eB)$ is always positive and increases with eB. The equations for the ℓ_{Ai} lines are given by Eq. (5). Note that each time that one of these lines is crossed from right to left some new LL's are populated. In fact, the crossing of ℓ_{A1} corresponds to the population of the d-quark state with $k = 1$, that of ℓ_{A2} to the *simultaneous* population of the u-quark state with $k = 1$ and d-quark state with $k = 2$, etc. The fact that the population of the u-quark state with a certain k coincides with the one of the d-quark state with $2k$ is simply due to the fact that (in modulus) the electric charge of the first is twice that of the second. Thus, those ℓ_{Ai} associated with odd i correspond to population of only one d-quark state while the ones with even i to the simultaneous population of a d-quark and a u-quark. Consequently larger effects are expected to happen when crossing the "even" ℓ_{Ai}. A similar phenomenon occurs when crossing the first order ℓ_{Ci} lines. This pattern can be particularly well observed in the upper panels of Fig. 7. Here one should keep in mind that the first transition (the one with the lowest μ) corresponds to the crossing of the ℓ_B line and, thus, should not be expected to follow the above-mentioned trend. Note that while in the B phase no quark state is populated, in both the C_0 and A_0 phases only the lowest Landau levels (LLL's) of the d- and u-quark are. It is also interesting to notice that for the parametrization $M_0 = 200$ MeV we are discussing each first order line ℓ_{Ci} appears to be naturally continued by the ℓ_{Ai} one. As we will see below, this correspondence is not so clear for larger values of M_0. To complete the description of the phase diagram for $M_0 = 200$ MeV we present some comments on the second order lines going from the points s_i to t_i, and which separate the A_i phase from the C_i one. The points on these lines obey relations that can be obtained by demanding that the quadratic coefficient of the Landau expansion of Eq. (3) vanishes. Although in general these relations can be only numerically given, the case for the line connecting s_0 to t_0 admits a simple analytical expression. It reads

$$\mu = \frac{1}{2^{2/3}}\sqrt{\frac{eB}{3\pi}}\exp\left[2\left(1 - \frac{g_c}{g}\right)\frac{\Lambda^2}{eB}\right] \tag{8}$$

with $g_c = \pi^2/N_c N_f$. Of course, the equation is valid for $eB(s_0) < eB < eB(t_0)$. The position of the critical point s_0 can be easily obtained by demanding that Eq. (8) and the relation $\mu = \frac{2}{3}eB$ are simultaneously satisfied. Note that the latter relation corresponds to the line ℓ_{C1} [see Eq. (5)]. On the other hand, to obtain the location of the critical point t_0, Eq. (8) has to be solved together with the relation satisfied by the first order line separating the B and C_0 phases, which follows from the condition $\Omega(\mu, eB, M(0, eB)) = \Omega(\mu, eB, 0)$. This procedure can be generalized so as to determine the precise position of the rest of the s_i and t_i critical points. However, due to the lack of simple analytical expressions for the equations involved, this has to be numerically done.

In the rest of this section we discuss how the eB-μ diagrams for cold quark matter evolve as we turn to parametrizations corresponding to the relevant range $300 < M_0 < 600$ MeV. Diagrams with several values of M_0 at intervals of 20 MeV are shown in Fig. 8. Only parametrizations up to $M_0 = 400$ MeV are explicitly displayed. As discussed below, beyond that value of M_0 the corresponding phase diagrams do not involve any qualitative new feature. Let us consider first the case $M_0 = 300$ MeV. As we see, there is a considerable simplification with respect to that of $M_0 = 200$ MeV. In fact, apart from the ever present B phase, only two massive phases exist in the relevant range of magnetic fields (very close to $eB = 0.01$ GeV^2 there is a very tiny region of C_2 phase which can hardly be seen in the figure). Thus, contrary to the case of $M_0 = 200$ MeV, there is a range of magnetic fields for which a first order transition can connect the C_i phase to some phases A_{i+m}, with $m > 1$. The fact that the C_1 phase is no longer simply connected can be understood as due to a "strangulation" of that region caused by the rise of the central part of the line connecting M to s_0. In fact, the strict correspondence between the first order line ℓ_{Ci} and the second order one ℓ_{Ai} (with the same i) mentioned above is lost here. Going now to the case $M_0 = 320$ MeV, only one sector of the C_1 phase (the one surrounded by the phases C_0, A_1 and A_2) shows up for $eB > 0.01$ GeV^2. Moreover, the C_0 phase gets smaller and is split into two pieces. It is interesting to note that slightly above $eB = 0.1$ GeV^2 two first order lines seem to touch at one

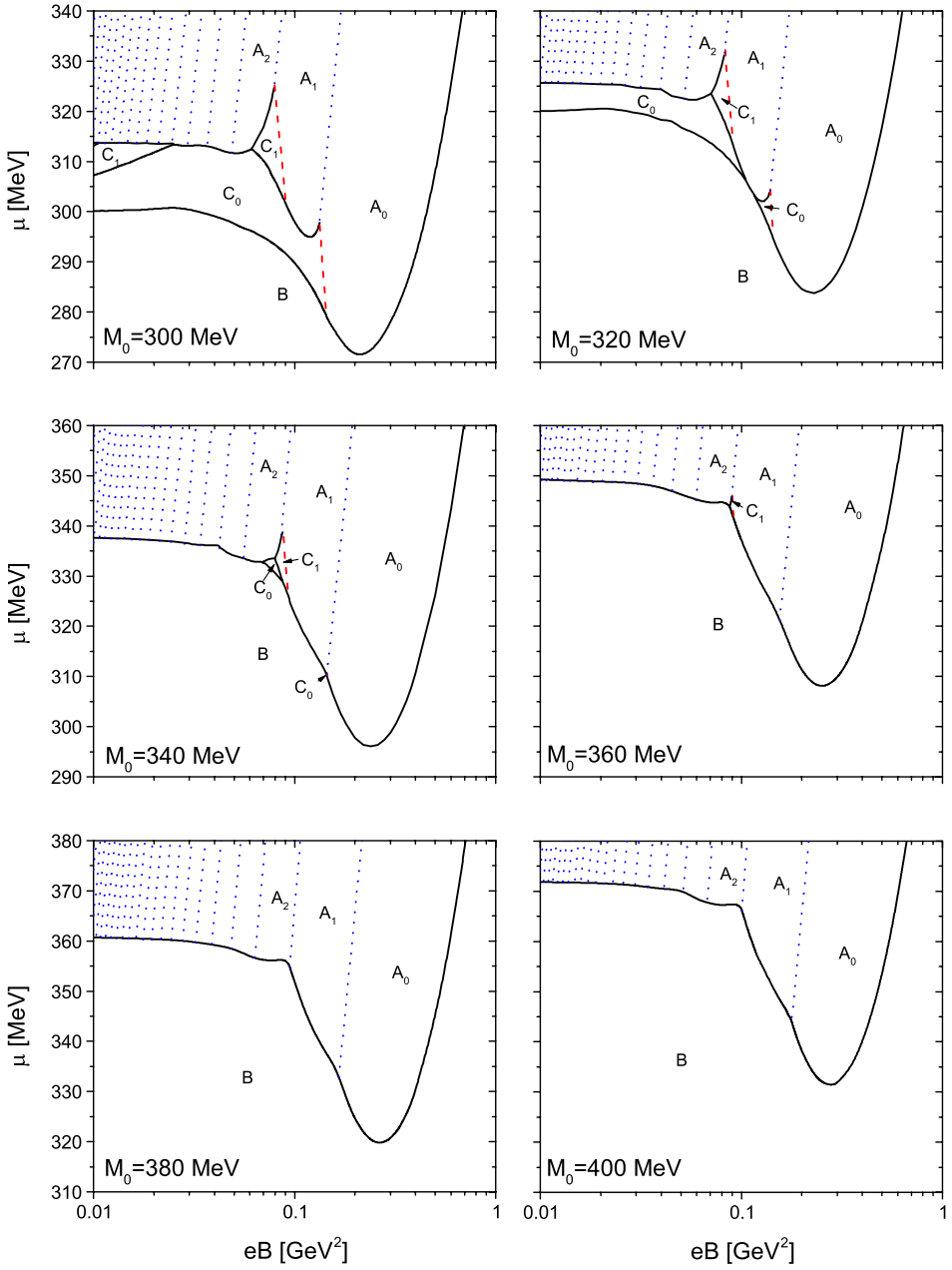

FIG. 8 (color online). Phase diagrams in the eB-μ plane in the chiral case and for various representative values of M_0. Full (black) lines represent first order phase transitions while dashed (red) lines to second order ones. Dotted (blue) lines correspond to the second order transitions which separate the different massless phases. Different phases are denoted as in Fig. 6.

single point. In fact this is exactly true for a somewhat lower value $M_0 = 319.2$ MeV. In any case, the existence of this particular meeting point might be worrisome since no more than three first order lines are expected to converge at one point. However, since only three different phases (B, C_0 and A_1) coexist at this point, this does not bring any contradiction with general statistical mechanical arguments. If M_0 is increased further to $M_0 = 340$ MeV only two small "islands" of C_0 remain: one (which can hardly be seen in the figure) is separated from the A_0 phase by a second order transition, and the other is fully surrounded by first order lines. In addition the C_1 region gets somewhat smaller. Note that since for this value of M_0 there is only one single first order transition in the limit of vanishing magnetic field (see Fig. 1), no other region of any C_i phase is expected to appear even for lower values of eB. For $M_0 = 360$ MeV the region C_1 becomes very tiny, and for $M_0 = 380$ MeV it is not present anymore. Note that from there on (see e.g. the diagram for $M_0 = 400$ MeV) the diagrams become very simple displaying only one first order phase transition for any arbitrary value of the magnetic field considered. Of course, in addition to it, we have the ℓ_{Ai} lines separating the

different A_i phases. The precise value at which the C_1 disappears can be determined by finding when the points s_1 and t_1 meet. Of course, this value coincides with that of $M_0(a)^{\rm hm}$ given in Eq. (6). Thus, for our choice $f_\pi^{\rm ch} = 90$ MeV, the parametrization beyond which the eB-μ diagram is particularly simple corresponds to $M_0 = 371.46$ MeV. We can also mention that the C_0 phase does not exist for parametrizations $M_0 > M_0(a)^{\rm lm}$.

It is interesting to address at this point the so-called "inverse catalysis effect" recently discussed in the literature [19]. This is usually related to a decrease of the critical chemical potential at intermediate values of the magnetic fields. Such a phenomenon is clearly observed for all the cases indicated in Fig. 8. In fact, we see that after staying fairly constant up to $eB \simeq 0.05$ GeV^2 the transition line ℓ_B bends down reaching a minimum at $eB \simeq 0.2$–0.3 GeV^2 after which it rises indefinitely with the magnetic field. This implies that, in general, there is some interval of values of the chemical potential for which an increase of the magnetic field at constant μ causes first a transition from the massive phase B to some massless phase A_i and afterwards from the massless phase A_0 back to massive phase B. This is clearly observed in Fig. 9 where we plot the behavior of M as a function of eB for several representative values of μ and $M_0 = 320$ and 400 MeV. An important feature not so often discussed in the literature (see however Ref. [14] for a brief comment on this) can also be noticed in the case of $M_0 = 320$ MeV: when the system is in a C_i phase there is an actual "inverse catalysis effect" in the sense that the order parameter for spontaneous chiral symmetry breaking (M or the chiral condensate) does decrease with the magnetic field while staying in the same phase. For example, in the case of $\mu = 300$ MeV (green dot-dashed line) there is first a "catalysis effect" while the system stays in the B phase, then at about $eB = 0.127$ GeV^2 there is a first order transition to the C_0 phase after which the "inverse catalysis effect" can be clearly observed. This situation proceeds up to $eB = 0.139$ GeV^2 where there is a second order transition to the A_0 phase. Eventually, at $eB = 0.394$ GeV^2 the system undergoes a new first order transition that brings it back to the B phase. In the case of $\mu = 310$ MeV (red dotted line) the situation is similar except for the fact that the intermediate transition is of first order. Finally, for $\mu = 321$ MeV (blue dashed line) the system is in the C_0 phase even for very small magnetic fields and, thus, the inverse catalysis effect is already present at low values of eB. At $eB = 0.074$ GeV^2 there is a first order transition to the C_1 phase after which the "inverse catalysis effect" can still be clearly observed. At $eB = 0.088$ GeV^2 there is a second first order transition to the A_1 where M vanishes and, finally, at $eB = 0.39$ GeV^2 there is a new first order transition to the B phase. Note that between the last two transitions there is a second order transition from the A_1 phase to the A_0 one which, of course, in the present chiral case does not produce any effect on the behavior of M as a function of eB.

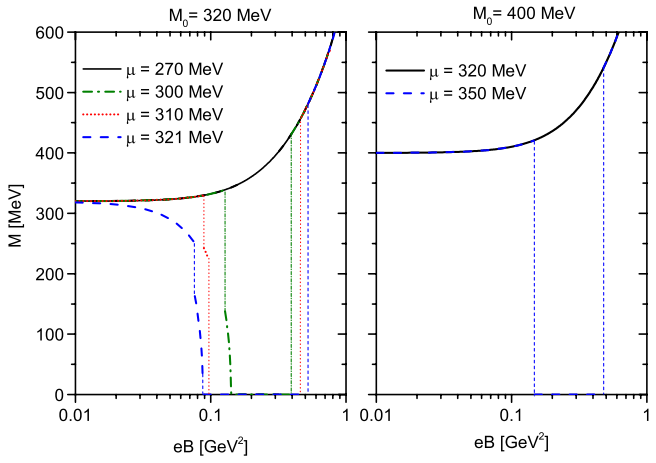

FIG. 9 (color online). Dressed quark mass M as a function of eB in the chiral case for several representative values of the chemical potential using the parameter sets associated with $M_0 = 320$ MeV (left panel) and $M_0 = 400$ MeV (right panel).

We conclude this section with a brief comment on the sometimes used LLL approximation. It is clear that such an approximation is well justified if only such Landau level is involved in the transitions under study. For example, for the parametrization $M_0 = 300$ MeV, this is the case for the lowest μ first order transition and the whole range of values of eB considered. However, the situation changes as M_0 increases. Already for $M_0 = 360$ MeV it can only be safely used to describe the transition between the B and C_0 phases, i.e. for rather large values of eB.

IV. FINITE CURRENT QUARK MASSES

The addition of a nonzero current mass to the problem brings along a few qualitative and quantitative differences. To begin with, there is no longer a universal character to the phase diagram: parameter sets associated with different values of f_π are not related among themselves through a scale change. In the rest of this work, we set $m_\pi = 138$ MeV and $f_\pi = 92.4$ MeV and choose a value of M_0 within the phenomenological range $300 \lesssim M_0 \lesssim 600$ MeV in order to fix the model parameters m_c, $g = G\Lambda^2$ and Λ. The resulting values as well as those associated with the corresponding chiral condensates are given in Appendix B.

For zero magnetic field, the M_0-μ phase diagram is qualitatively similar to the one corresponding to the chiral case (see Fig. 1) except for the fact that the highest μ second order transitions occurring for $M_0 < M_0(b)$ become smooth crossovers here. For the values of f_π and m_π given above, we find $M_0(a) = 361.2$ MeV and $M_0(b) = 300.1$ MeV.

We turn now to the case of finite magnetic field. Before presenting the actual phase diagrams we will discuss the main qualitative differences introduced by the existence of finite current quark mass. We start by the second order lines which separate the different A_i phases in the chiral

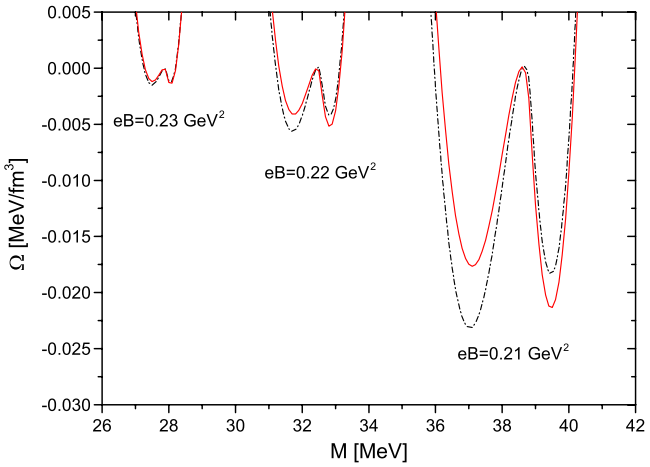

FIG. 10 (color online). Thermodynamical potential as a function of M for some representative values of eB. In each case we have subtracted the value of the thermodynamical potential at the intermediate maximum so as to be able to include all the cases in the same plot. Red full lines (black dot-dashed lines) correspond to a value of chemical potential slightly above (below) the critical value.

case, and whose equations are given in Eq. (5). Let us recall that the corresponding critical chemical potentials are the values at which new LL's contribute to the sum in the last line of Eq. (3) for $M = 0$. In the case of finite quark masses, although M never vanishes we can still define the value of the chemical potential at which new LL's are populated, i.e. the one that satisfies the condition $\mu = \sqrt{M^2 + 2kc_f eB/3}$. As it turns out, in all the cases under study we found that for a given value of eB there is no second order transition located at this chemical potential but a (weak) first order one in its vicinity, the transition becoming weaker as the critical μ increases. Namely, the second order $\ell_{\mathrm{A}i}$ lines present in the chiral case become first order here, being signaled by very small jumps in the dressed mass. The situation is illustrated in Fig. 10 where we plot the thermodynamical potential as a function of M for some representative values of eB. In each case, we have chosen one value of μ above the critical chemical potential and the other one below. Moreover, in each case we have subtracted the value of the thermodynamical potential at the intermediate maximum so as to be able to include all the cases in the same plot. Figure 10 clearly displays the existence of two solutions on either side of the point at which the condition mentioned above is satisfied, and how one of them becomes the absolute minimum depending on whether μ is below (black full line) or above (red dot-dashed line) its critical value. The decrease of the jump in mass as eB (and, thus, the critical chemical potential) increases can also be observed in Fig. 10. Since for finite

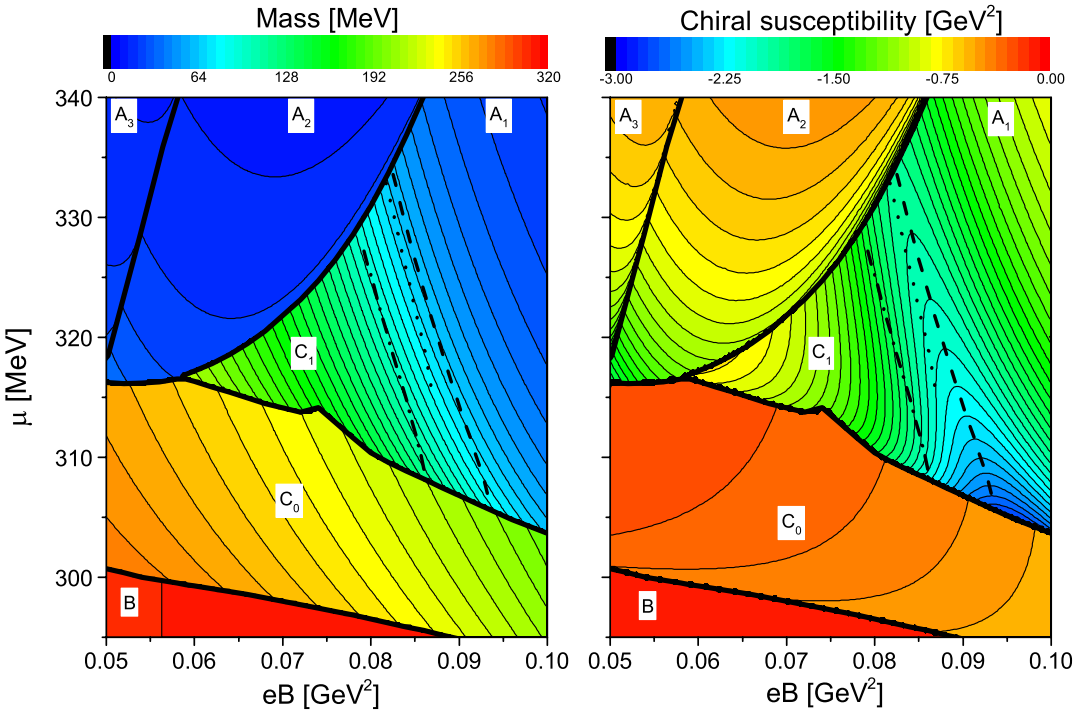

FIG. 11 (color online). Contour plots of the dressed mass (left panel) and the chiral susceptibility (right panel) as functions of μ and eB. Parameters are as in the chiral case for $M_0 = 300$ MeV but with $m_c = 1$ MeV. Full (black) lines represent first order phase transitions. The different definitions discussed in the text are used to obtain the crossover transition lines: Def. (i) (peak of dM/dB) is represented by dot-dashed line, Def. (ii) (peak of χ_{ch} as a function of eB) by a dashed line and Def. (iii) (peak of χ_{ch} as a function of μ) by a dotted line. Def. (iv) corresponds to the line of "slowest descent" from the absolute peak of the chiral susceptibility (dark blue region in right panel) which basically coincides with that of Def. (ii). Different phases are denoted as in Fig. 6.

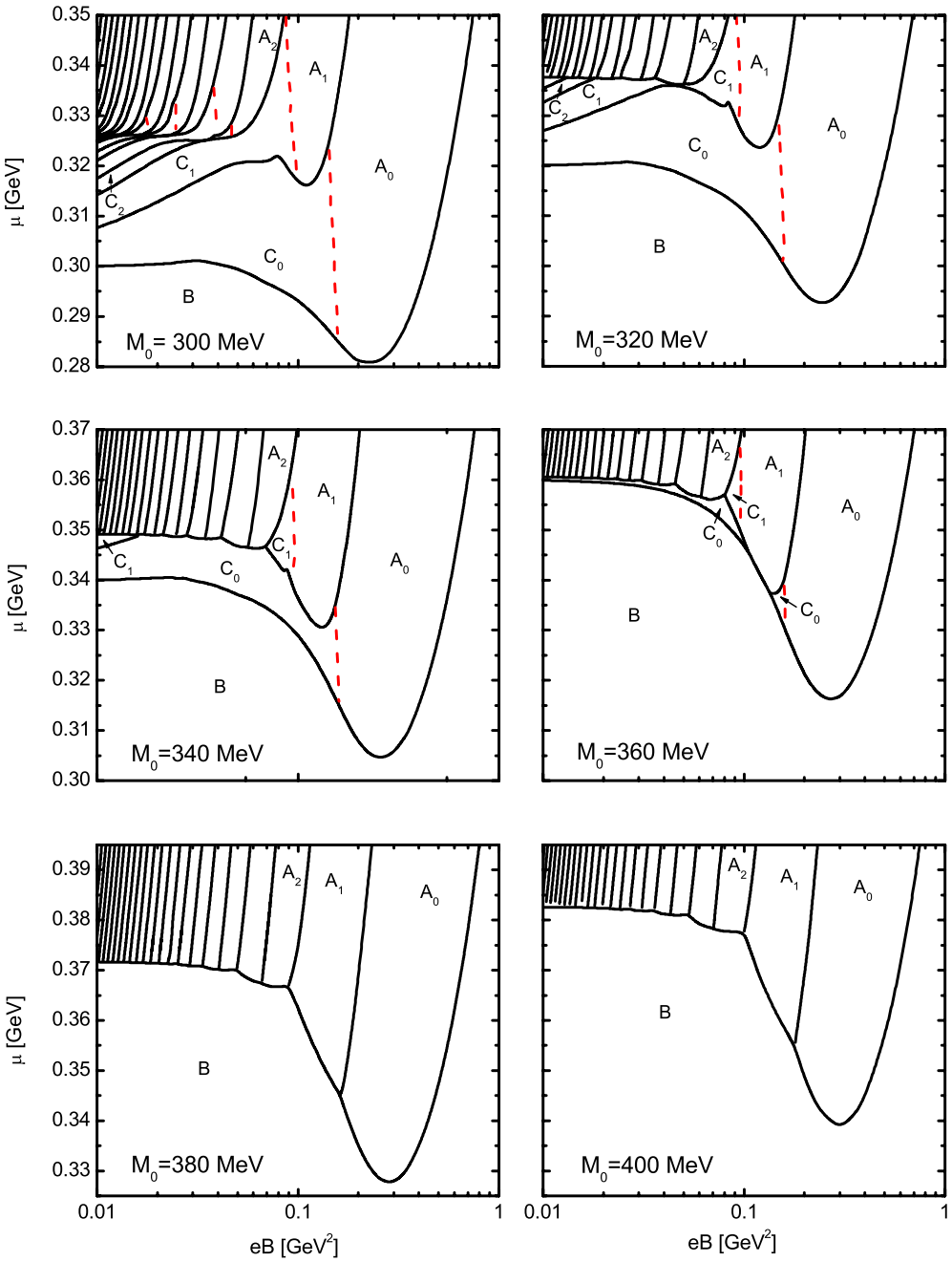

FIG. 12 (color online). Phase diagrams in the eB-μ plane in the case of finite current quark masses and for various representative values of M_0. Full (black) lines represent first order phase transitions while dashed (red) lines crossover ones. Different phases are denoted as in Fig. 6.

current quark masses the different A_i phases are separated by first order lines (in the same way as different C_i phases are), it is no longer possible to distinguish between ℓ_{Ai} and ℓ_{Ci} lines as done in the chiral case: one simply has a single continuous first order line that plays their role.

We turn now to the fate of the transition lines that separate the phases C_i from the A_i ones, and which are of second order in the chiral case. For finite current quark masses these transitions become smooth crossovers. Consequently, as already mentioned in Sec. III, there is not a unique way to define their position. In the present case, considering the peak of the derivative of M with respect to μ or B gives rise to two possible prescriptions. As it happens, however, due to the particular form of the transition lines (rather parallel to the μ axis as one can expect from the chiral case, see Fig. 8) we find that in general there is no peak of $dM/d\mu$. Thus, we are only left with the second possibility that we denote Def. (i). For basically the same reason, the transition line defined as the position of the peaks of the chiral susceptibility when plotted as a function of eB at fixed μ [denoted

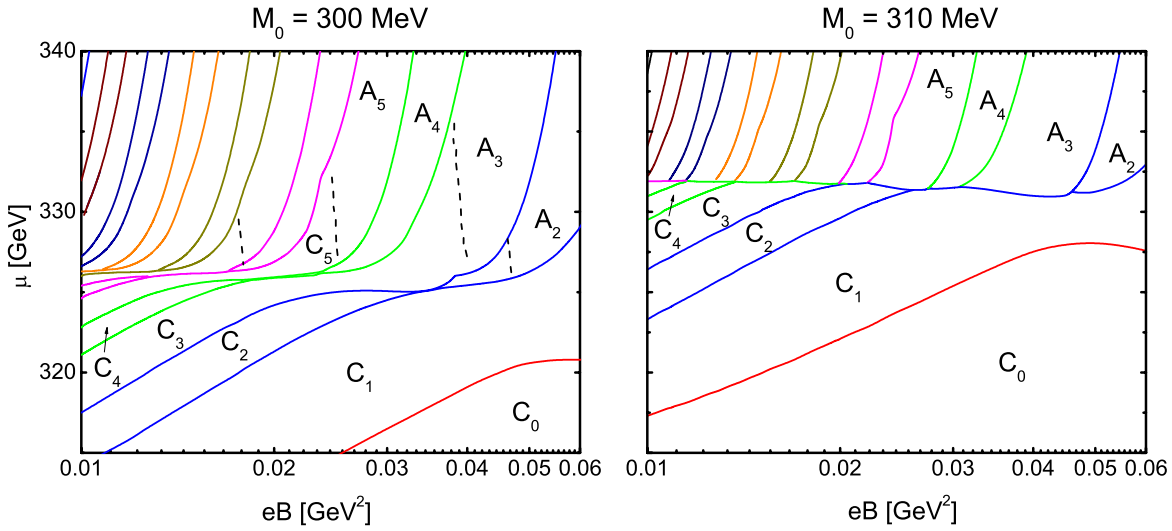

FIG. 13 (color online). Detail of the eB-μ phase diagram in the case of finite current quark masses for $M_0 = 300$ MeV (left panel) and $M_0 = 310$ MeV (right panel). Different phases are denoted as in Fig. 6.

Def. (ii)] do not coincide, in general, with the one that follows from the alternative possibility [denoted Def. (iii)], i.e. the peaks of the chiral susceptibility when plotted as a function of μ at fixed eB. Moreover, in the latter case the transition line tends to be washed away when the current quark mass is varied from $m_c = 0$ to its corresponding physical value. To avoid this dependence on the somewhat ad-hoc chosen direction in the eB-μ plane one can define the transition line as the ridge occurring in the chiral susceptibility when regarded as a two dimensional function of eB and μ. Mathematically, it can be defined by using for each value of the susceptibility (starting from its maximum value in the given region) the location of the points at which the gradient in the eB-μ plane is smaller. We denote this as Def. (iv). The situation is illustrated in Fig. 11 where we plot the contour lines corresponding to M (left panel) and the chiral susceptibility (right panel) for the case in which Λ and g take the values associated to the chiral case with $M_0 = 300$ MeV but m_c is arbitrarily set to $m_c = 1$ MeV. While nonphysical, for this parameter set it is possible to use all the alternative ways to define the transition lines mentioned above (in particular, that associated with the peak of $d\chi_{\rm ch}/d\mu$ which rapidly disappears as m_c increases). In this way one can obtain some measure of the ambiguity this introduces in the location of the transition line. In Fig. 11 the thick dot-dashed lines correspond to Def. (i), the dashed line to Def. (ii) and the dotted line to Def. (iii). From the left panel of this figure it is quite clear that the latter definition leads to a transition line which basically coincides with the one obtained from Def. (iv), which in turn corresponds to the line of "slowest descent" from the absolute peak of the chiral susceptibility (darker blue region). Although some alternative definitions are still possible (e.g. the contour line in the susceptibility diagram that, at the contact point, is tangent to the first order line that separates the C_1 or A_1 phases from the A_2) we see that the different definitions lead to qualitatively similar results. Thus, in what follows we will use Def. (iv) keeping in mind that to ensure the real existence of the transition line one should be able to define it in at least more than one way. This requires that Def. (iv) must be complemented with the condition that on each side of the curve there should exist at least one region such that there is a maximum in the susceptibility for an arbitrary path connecting both regions. As a corollary of this discussion we note that the location of the critical points equivalent to the points s_i and t_i discussed in the previous section is also subject to definition ambiguities.

The phase diagrams in the eB-μ plane for different values of M_0 are presented in Fig. 12. Apart from the particular features just discussed, we observe that the general trend is similar to the one of the chiral case shown in Fig. 8: For low M_0 values there are several different transitions that coalesce into fewer transitions as M_0 is increased. Moreover, while several crossovers between C_i and A_i phases are still present for the set $M_0 = 300$ MeV, they continue to exist from $M_0 = 320$ MeV until $M_0 = 360$ MeV only for $i = 0, 1$. It would seem that a phase diagram for a given M_0 in the chiral case is always similar to another one in the nonchiral case with larger M_0. In particular, for finite quark masses the value of M_0 above which there is a unique transition is 375.9 MeV. It interesting to note that in this case the C_0 phase (in particular the piece completely surrounded by first order transition lines) is the last one to disappear. In fact, the C_1 phase ceases to exist for values of M_0 slightly above 360 MeV.

The way in which curves merge together as M_0 increases is qualitatively similar to the chiral case. This is shown in Fig. 13 where we display a detail of the eB-μ diagram for $M_0 = 300$ MeV (left panel) and $M_0 = 310$ MeV (right panel). We see that the curves develop a flat cubic-like

region, through which they come into contact. A transition curve that is nearly independent of the chemical potential is eventually formed from these flat regions. From the original curves, the vertical parts with higher chemical potential (i.e. those separating the A_i phases) continue to exist as M_0 is increased, while the lower chemical potential parts of the curves tend to move to lower magnetic field values and eventually disappear. In Fig. 13 it is also quite clearly seen that the curves join in pairs, transition curves being colored in the figure as to indicate which curves join between themselves. For example, the first line to the right, corresponding to the simultaneous population of the second d-quark LL and the first u-quark LL, merges with the following curve which corresponds to the population of the third d-quark LL.

We end this section by discussing the inverse catalysis effect for the case in which a finite current mass is present. In Fig. 14, we display the behavior of the mass as a function of magnetic field for several chemical potentials, and the $M_0 = 320$ MeV and $M_0 = 400$ MeV parameter sets. The complex phase structure for the $M_0 = 320$ MeV case accounts for the different possible behaviors depending on the chemical potential. For $\mu = 290$ MeV, the system is in the B phase for the whole range of magnetic fields, and the catalysis effect is clearly seen. For $\mu = 310$ MeV, a similar behavior is seen, except for a middle section where the system passes through a C_0 phase and an A_0 phase before returning to the vacuum phase again. As opposed to the chiral case, the transition from C_0 to A_0 is not particularly noticeable since at most the transition is signaled by a peak in the susceptibility or the derivatives in the order parameter as already discussed. In this region of the curve, as well as in the rest of the following curves, the effect of inverse catalysis is also present. In fact, it is absolutely dominant except for barely noticeable regions in the A_i phases for the $\mu = 340$ MeV curve, and we can conclude that within phases

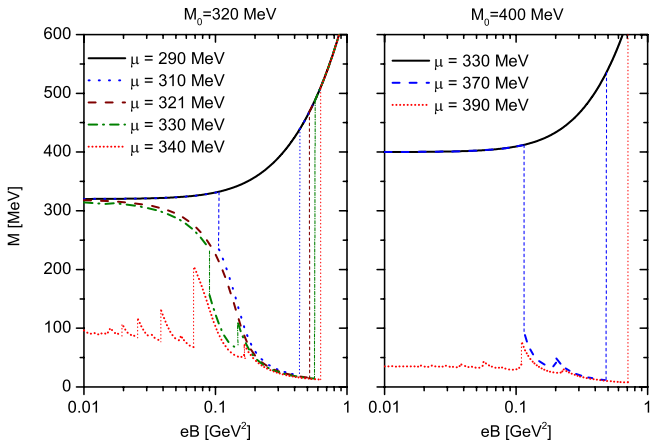

FIG. 14 (color online). Dressed quark mass M as a function of eB for several representative values of the chemical potential using the parameter sets associated with $M_0 = 320$ MeV (left panel) and $M_0 = 400$ MeV (right panel).

with nonzero quark density, the value of M is typically a decreasing function of the magnetic field, while catalysis occurs principally in the vacuum phase. In particular, for $\mu = 321$ MeV, the phase remains in C_0 for a significant range of magnetic fields and the mass decreases continuously. Paying attention to the cases $\mu = 330$ MeV and $\mu = 340$ MeV, we will also note that when we move to a phase of increasing i, so as to populate new LL's, the discontinuity will be toward a lower mass, while if i decreases in the transition so as to leave a formerly occupied Landau level empty, the jump will be toward a higher mass.

V. SUMMARY AND CONCLUSIONS

In this work we have considered the phase structure of magnetized cold quark matter in the framework of the two-flavor Nambu-Jona-Lasinio models. As is well known, even in the simplest version of these models there is a rather broad range of phenomenologically acceptable values for the corresponding model parameters. Thus, we have performed a detailed analysis of how the character and location of the different types of phase transitions depend on the chosen parametrization. As is frequently done in the literature, we have specified each parametrization by the associated value of the dressed quark mass in the vacuum at vanishing magnetic field M_0, with the phenomenological range given by $300 \lesssim M_0 \lesssim 600$ MeV [21]. We have first discussed the simpler situation in which the chiral limit is taken. In this case the phase structure is basically dictated by the ratio M_0/f_π^{ch}. For $M_0/f_\pi^{\mathrm{ch}} > 4.127$ such structure is particularly simple since only one single first order transition line ℓ_{B} exists. This line separates the vacuum phase B from the ones in which a certain number of Landau levels associated with massless u- and d-quarks are populated. Following Ref. [10] we denote the latter ones as A_i phases. They are separated by second order transition lines that we called ℓ_{A_i}. On the other hand, for $M_0/f_\pi^{\mathrm{ch}} < 4.127$ the phase diagram is more complex since additional first phase order and second order transition lines appear as M_0 decreases. In particular, there appear new phases C_i in which chiral symmetry is only partially restored. Namely, for a given magnetic field the corresponding dressed mass is smaller than its vacuum value and depends on the chemical potential. It is important to stress that, for a typical value $f_\pi^{\mathrm{ch}} = 90$ MeV, the parametrization below which these new phases and transition lines appear corresponds to $M_0 = 371.46$ MeV, a value which is well inside the phenomenological acceptable range quoted above.

When a finite current mass is included in the model there are some changes, but the general structure of the eB-μ phase diagram remains the same, with a particular M_0 diagram in the chiral case typically very similar to another one with larger M_0 in the nonchiral case. In particular, a slightly higher value $M_0 = 375.9$ MeV is required for the passage from the broken symmetry phase to the restored phases A_i to occur in one single transition. As in the chiral

case, below this critical M_0 value several transitions are needed to move from the vacuum phase B to the chiral symmetry restored phases A_i, if chemical potential is increased at constant magnetic field. One of the most notable qualitative modifications induced by the presence of a finite quark mass is related to the character of the transitions between the A_i phases: while in the nonchiral case the transitions are of first order, signaled by a jump both in the density and the dressed mass, in the chiral case the order parameter is zero in all of these phases and the transition is second order and signaled by a discontinuous derivative of the quark density. The transitions between a C_i phase and the corresponding A_i phase are also different, being second order transitions in the chiral case and smooth crossovers when current mass is finite. Several definitions for the location of the crossover transitions were studied, finding in general that even though the different definitions introduce certain ambiguity as to the exact location of the transition, in all studied cases they agree on whether the transition actually exists or not. As well, in what respects to their tendency to disappear as M_0 increases, these crossovers behave similarly to their second order analogues occurring in the chiral case.

The behavior of the dressed mass for a constant μ in response to magnetic field was studied as well for both the chiral and nonchiral cases, resulting in different effects depending on the phase. On the one hand, the increase in dressed mass with magnetic field, known as magnetic catalysis, was principally seen in the vacuum phase B, where symmetry is fully broken, in both chiral and nonchiral cases. On the other hand, phases with nonzero quark density and finite dressed mass (C_i phases in the chiral case, and C_i and A_i in the nonchiral case) showed a dominant decrease in the dressed mass as magnetic field increased. This can be taken as a manifestation of inverse magnetic catalysis usually associated with a decrease of the critical chemical potential at intermediate values of the magnetic fields [19]. It should be noted that these continuous drops in the mass occurred within single phases, and that discontinuous jumps occurred whenever a new phase with a different amount of occupied Landau levels was reached.

Throughout this work only the simplest version of the two flavor NJL with maximum flavor mixing has been considered. It is clear that the parametrization dependence of the phase structure of magnetized cold quark matter as described by possible extensions of the model which incorporate the effect of different amounts of flavor mixing [14], color superconductor channels [15,17,18], vector interactions [28], strangeness degrees of freedom [29], etc. is interesting and certainly deserves further investigation. Of course, the analysis of how the phase structure of magnetized quark matter at finite temperature depends on the model parametrization should also be addressed [30]. In this respect, however, it is important to mention that the model extensions that incorporate the effect of the Polyakov loop reduce, in the low temperature region, to the type of model studied here. Finally, studying the parameter dependence of the predictions for the properties of the pion and sigma meson in the presence of intense magnetic fields [31,32] will be useful as well.

ACKNOWLEDGMENTS

Fruitful discussions with Marcus B. Pinto, Debora P. Menezes and Daniel Gomez Dumm are greatly acknowledged. This work has been partially funded by CONICET (Argentina) under Grant No. PIP 00682 and by ANPCyT (Argentina) under Grant No. PICT-2011-0113.

APPENDIX A: PARAMETRIZATION IN THE CHIRAL CASE

In this appendix we provide some details of the way in which the parameters are determined in the chiral limit. In this case the model has only two parameters: the coupling constant G and the 3D cutoff Λ. In order to work along "a line of constant physics" we choose to determine them so as to reproduce a certain value of $f_\pi^{\rm ch}$, taking the dressed mass M_0 as a free parameter which takes values within a typical range 200–600 MeV. The set of equations to be

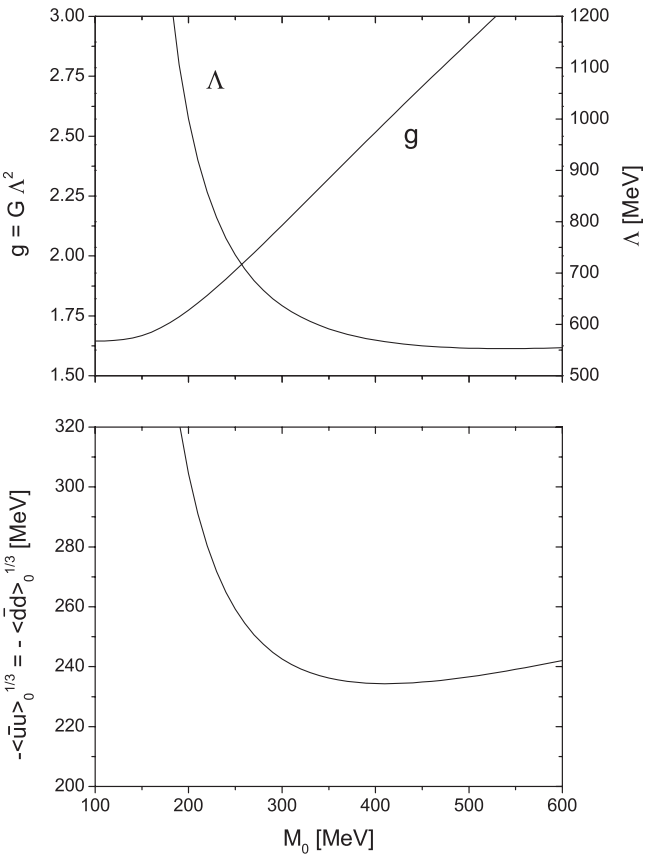

FIG. 15. Upper panel: Cutoff parameter Λ and dimensionless coupling constant g as functions of the dressed quark mass M_0. Lower panel: Chiral quark condensate as a function of the dressed quark mass M_0.

satisfied by the dimensionless coupling $g = G\Lambda^2$ and the cutoff Λ are the $T = \mu = 0$ gap equation

$$g_c = g\, f\left(\frac{M_0}{\Lambda}\right) \tag{A1}$$

together with

$$(f_\pi^{\rm ch})^2 = \frac{N_c}{2\pi^2}\Lambda^2\left[\frac{M_0^2}{\sqrt{M_0^2+\Lambda^2}} - f\left(\frac{M_0}{\Lambda}\right)\right]. \tag{A2}$$

The second equation corresponds to the expression for f_π in the chiral limit. Moreover, $g_c = \pi^2/(N_c N_f)$ is the critical dimensionless coupling above which the gap equation has nontrivial solutions and

$$f(x) = \sqrt{1+x^2} - x^2 \ln\left(\frac{1+\sqrt{1+x^2}}{x}\right). \tag{A3}$$

The numerical results for g and Λ as functions of M_0 are shown in the upper panel of Fig. 15. In the lower panel we display the values of the quark condensates associated with the corresponding values of the parameters. Here, we have chosen a typical value for $f_\pi^{\rm ch} = 90$ MeV. Note, however, that since in the chiral limit $f_\pi^{\rm ch}$ is the only dimensionful quantity in the problem any dimensionful quantity (expressed in natural units) has to be the product of some $f_\pi^{\rm ch}$-independent constant multiplied by some power of it. This means that if, for example, in the lower panel of Fig. 15 we divide the quantities in both axes by $f_\pi^{\rm ch} = 90$ MeV the resulting curve is universal in the sense that it does not depend on the chosen value of $f_\pi^{\rm ch}$. Of course, some extra dependence on the procedure used to regularize the UV divergencies might still exist.

TABLE I. Parameter sets for the nonchiral case.

M_0 MeV	m_c MeV	$g = G\Lambda^2$	Λ MeV	$-\langle\bar{u}u\rangle_0^{1/3}$ MeV
300	5.175	2.062	664.4	250.8
310	5.307	2.099	651.0	248.7
320	5.419	2.136	639.5	246.9
340	5.595	2.212	620.9	244.3
360	5.716	2.288	606.8	242.5
380	5.792	2.364	596.1	241.4
400	5.833	2.440	587.9	240.9

APPENDIX B: PARAMETRIZATION IN THE FINITE QUARK CASE

In this Appendix we give the model parameters used in our calculations of Sec. IV, i.e. for the nonchiral case. They are listed in Table I. As stated in the main text the are determined so as to reproduce the physical values $m_\pi = 138.0$ MeV and $f_\pi = 92.4$ MeV for a chosen value of dressed quark mass M_0 within the phenomenological range $300 \lesssim M_0 \lesssim 600$ MeV [21]. The resulting values of the condensates $-\langle\bar{u}u\rangle_0^{1/3} = -\langle\bar{d}d\rangle_0^{1/3}$ are also given. We remind here that the limits extracted from sum rules are $190\ \text{MeV} < -\langle u\bar{u}\rangle_0^{1/3} < 260\ \text{MeV}$ at a renormalization scale of 1 GeV [22], while typical lattice calculations yield $-\langle u\bar{u}\rangle_0^{1/3} = 231 \pm 8 \pm 6$ MeV [23] (see e.g. Ref. [24] for some other lattice results).

[1] D. Kharzeev, K. Landsteiner, A. Schmitt, and H.-U. Yee, Lect. Notes Phys. **871**, 1 (2013).

[2] D. E. Kharzeev, L. D. McLerran, and H. J. Warringa, Nucl. Phys. **A803**, 227 (2008); V. Skokov, A. Y. Illarionov, and V. Toneev, Int. J. Mod. Phys. A **24**, 5925 (2009); V. Voronyuk, V. D. Toneev, W. Cassing, E. L. Bratkovskaya, V. P. Konchakovski, and S. A. Voloshin, Phys. Rev. C **83**, 054911 (2011).

[3] R. C. Duncan and C. Thompson, Astrophys. J. **392**, L9 (1992); C. Kouveliotou *et al.*, Nature (London) **393**, 235 (1998).

[4] S. Borsanyi, Z. Fodor, C. Hoelbling, S. D. Katz, S. Krieg, C. Ratti, and K. K. Szabó (Wuppertal-Budapest Collaboration), J. High Energy Phys. 09 (2010) 073; A. Bazavov, T. Bhattacharya, M. Cheng, C. DeTar, H. T. Ding, S. Gottlieb, R. Gupta, and P. Hegde *et al.*, Phys. Rev. D **85**, 054503 (2012).

[5] F. Karsch and E. Laermann, in *Quark Gluon Plasma 3*, edited by R. C. Hwa *et al.* (World Scientific, Singapore, 2004), p. 1.

[6] E. S. Fraga, Lect. Notes Phys. **871**, 121 (2013).

[7] R. Gatto and M. Ruggieri, Lect. Notes Phys. **871**, 87 (2013).

[8] V. P. Gusynin, V. A. Miransky, and I. A. Shovkovy, Phys. Rev. Lett. **73**, 3499 (1994); **76**, 1005(E) (1996).

[9] G. S. Bali, F. Bruckmann, G. Endrodi, Z. Fodor, S. D. Katz, S. Krieg, A. Schafer, and K. K. Szabo, J. High Energy Phys. 02 (2012) 044; G. S. Bali, F. Bruckmann, G. Endrodi, Z. Fodor, S. D. Katz, and A. Schafer, Phys. Rev. D **86**, 071502 (2012).

[10] D. Ebert, K. G. Klimenko, M. A. Vdovichenko, and A. S. Vshivtsev, Phys. Rev. D **61**, 025005 (1999).

[11] D. Ebert and K. G. Klimenko, Nucl. Phys. **A728**, 203 (2003).

[12] T. Inagaki, D. Kimura, and T. Murata, Prog. Theor. Phys. **111**, 371 (2004).

[13] D. P. Menezes, M. Benghi Pinto, S. S. Avancini, A. Perez Martinez, and C. Providencia, Phys. Rev. C **79**, 035807 (2009).

[14] J. K. Boomsma and D. Boer, Phys. Rev. D **81**, 074005 (2010).

[15] S. Fayazbakhsh and N. Sadooghi, Phys. Rev. D **82**, 045010 (2010).
[16] G. N. Ferrari, A. F. Garcia, and M. B. Pinto, Phys. Rev. D **86**, 096005 (2012).
[17] E. J. Ferrer and V. de la Incera, Lect. Notes Phys. **871**, 399 (2013).
[18] T. Mandal, P. Jaikumar, and S. Digal, arXiv:0912.1413; T. Mandal and P. Jaikumar, Phys. Rev. C **87**, 045208 (2013).
[19] F. Preis, A. Rebhan, and A. Schmitt, J. High Energy Phys. 03 (2011) 033; Lect. Notes Phys. **871**, 51 (2013).
[20] U. Vogl and W. Weise, Prog. Part. Nucl. Phys. **27**, 195 (1991); S. Klevansky, Rev. Mod. Phys. **64**, 649 (1992); T. Hatsuda and T. Kunihiro, Phys. Rep. **247**, 221 (1994); M. Buballa, Phys. Rep. **407**, 205 (2005).
[21] M. Buballa, Phys. Rep. **407**, 205 (2005).
[22] H. G. Dosch and S. Narison, Phys. Lett. B **417**, 173 (1998).
[23] L. Giusti, F. Rapuano, M. Talevi, and A. Vladikas, Nucl. Phys. **B538**, 249 (1999).
[24] C. McNeile, Phys. Lett. B **619**, 124 (2005).
[25] M. Buballa, Nucl. Phys. **A611**, 393 (1996).
[26] K. G. Klimenko and A. S. Vshivtsev, Pis'ma Zh. Eksp. Teor. Fiz. **64**, 313 (1996) [JETP Lett. **64**, 338 (1996)].
[27] A. S. Vshivtsev, V. C. Zhukovsky, and K. G. Klimenko, Zh. Eksp. Teor. Fiz. **111**, 1921 (1997) [J. Exp. Theor. Phys. **84**, 1047 (1997)].
[28] R. Z. Denke and M. B. Pinto, Phys. Rev. D **88**, 056008 (2013).
[29] D. P. Menezes, M. Benghi Pinto, S. S. Avancini, and C. Providencia, Phys. Rev. C **80**, 065805 (2009).
[30] P. G. Allen and N. N. Scoccola, in *Proceedings of Compact Stars in the QCD Phase Diagram III, Guarujá, Brasil, 2012*, eConf C121212 (2013).
[31] V. P. Gusynin, V. A. Miransky, and I. A. Shovkovy, Phys. Lett. B **349**, 477 (1995); Nucl. Phys. **B462**, 249 (1996).
[32] S. Fayazbakhsh, S. Sadeghian, and N. Sadooghi, Phys. Rev. D **86**, 085042 (2012).